International Journal of Neural Systems, Vol. 26, No. 1 (2016) 1550031 (19 pages)

DOI: 10.1142/S0129065715500318

A General Approach for Quantifying Nonlinear Connectivity in the Nervous System Based on Phase Coupling

Yuan Yang* and Teodoro Solis-Escalante
Department of Biomechanical Engineering, Delft University of Technology
Delft 2628 CD, The Netherlands
**y.yang-2@tudelft.nl*

Jun Yao
Department of Physical Therapy and Human Movement Sciences
Feinberg School of Medicine, Northwestern University
Chicago, IL 60611, USA

Andreas Daffertshofer
Faculty of Human Movement Sciences, VU University Amsterdam
Amsterdam, 1081 BT, The Netherlands

Alfred C. Schouten
Department of Biomechanical Engineering, Delft University of Technology
Delft 2628 CD, The Netherlands

MIRA Institute for Biomedical Technology and Technical Medicine
University of Twente, Enschede, 7500 AE, The Netherlands

Frans C. T. van der Helm†
Department of Biomechanical Engineering, Delft University of Technology
Delft 2628 CD, The Netherlands
F.C.T.vanderHelm@tudelft.nl

Accepted 5 August 2015
Published Online 25 September 2015

Interaction between distant neuronal populations is essential for communication within the nervous system and can occur as a highly nonlinear process. To better understand the functional role of neural interactions, it is important to quantify the nonlinear connectivity in the nervous system. We introduce a general approach to measure nonlinear connectivity through phase coupling: the multi-spectral phase coherence (MSPC). Using simulated data, we compare MSPC with existing phase coupling measures, namely $n:m$ synchronization index and bi-phase locking value. MSPC provides a system description, including (i) the order of the nonlinearity, (ii) the direction of interaction, (iii) the time delay in the system, and both (iv) harmonic and (v) intermodulation coupling beyond the second order; which are only partly revealed by other methods. We apply MSPC to analyze data from a motor control experiment, where subjects performed isotonic wrist flexions while receiving movement perturbations. MSPC between the perturbation, EEG and EMG was calculated. Our results reveal directional nonlinear connectivity in the afferent and efferent pathways, as well as the time delay (43 ± 8 ms) between the perturbation and the brain response. In conclusion, MSPC is a novel approach capable to assess high-order nonlinear interaction and timing in the nervous system.

Keywords: Phase coupling; nonlinear interaction; motor control; time delay; EEG; EMG.

†Corresponding author.

1. Introduction

The human nervous system is a highly cooperative network comprised of different groups of neurons. Exchange of information between neuronal populations is essential for the nervous system to coordinate neuronal groups and integrate their functions. Neural synchronization between distant, but functionally related, neuronal groups has been shown for many tasks including motor control and sensory integration.[1–5] Many studies investigating long-range neural synchronization have focused on the linear interaction between neuronal assemblies using connectivity measures like linear coherence.[6–9] However, several studies indicate that neural connectivity can be highly nonlinear.[2,10–13] Nonlinear interactions enable rich and context-sensitive communications in the nervous system and play an important role in perceptual synthesis and sensorimotor integration.[14,15]

Linear interaction refers to neural synchronization at the same frequency (e.g. $f_1 \rightarrow f_1$), whereas nonlinear interaction can refer to synchronization between harmonic (e.g. $f_1 \rightarrow 3f_1$) and/or intermodulation (e.g. $\{f_2, f_3\} \rightarrow 2f_2 - f_3$) frequencies (see Fig. 1. for different input–output interactions in linear and nonlinear systems). In the nervous system, *harmonic interaction*, where the output frequency is a multiple of the input frequency, is related to resonant behavior of neural processing[16,17]; whereas *intermodulation*, where multiple input frequencies can contribute to one output frequency, is linked to functional integration.[18–20]

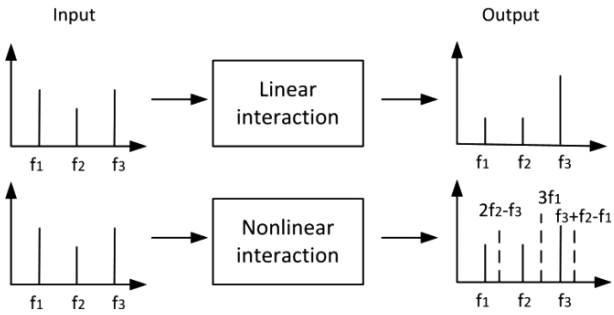

Fig. 1. Scheme of linear and nonlinear interactions in the frequency domain. With a linear interaction, the output contains spectral components at the same frequencies as the input (solid lines), while a nonlinear interaction can generate spectral components in the output at nonstimulated frequencies (dashed lines), such as the harmonic (e.g. $3f_1$) and intermodulation (e.g. $2f_2 - f_3, f_3 + f_2 - f_1$) frequencies.

Although nonlinear interaction between neurophysiological signals can occur purely in phase[a,3,21] or involving amplitude[22,23] (e.g. amplitude correlation[24,25] and phase–amplitude coupling[26,27]), we favor the assessment of nonlinear interaction through pure phase coupling, because it is thought to directly reflect the relative timing of neural activity.[28] Several methods can be used to detect harmonic or second-order intermodulation (i.e. $\{f_1, f_2\} \rightarrow f_1 + f_2$) phase coupling, exclusively (for review, see Refs. 24, 28 and 29). The aim of this paper is to introduce a general approach that allows for quantifying nonlinear phase coupling including both harmonic and intermodulation (also beyond the second order), so as to estimate the directional nonlinear connectivity and time delay in the nervous system.

In terms of existing nonlinear phase coupling measures, bicoherence and its variants, i.e. high-order spectra methods,[11,30–34] are often used to study the nervous system in both animals[35,36] and humans.[37–41] Bicoherence has been proposed to quantify the second-order phase coupling (also called quadratic phase coupling, QPC) among three frequencies, i.e. a pair of frequencies $\{f_1, f_2\}$ is coupled with a third frequency f_3, which is the sum of these two frequencies (i.e. $f_3 = f_1 + f_2$). However, bicoherence and also other methods based on high-order spectra mix phase and amplitude relationships between signals[29,42]; which is similar to the case of linear coherence.[43,44] Thus a nonstationary amplitude ratio between frequencies may lead to spurious estimation of phase coupling. This bias on phase coupling estimation will further result in unreliable estimation of time delay, when using bicoherence to estimate the phase lag between frequencies.[37] Given the nonstationary properties of neurophysiological signals such as the electroencephalogram (EEG),[45] bicoherence is not an ideal measure to assess "pure" phase coupling (as well as time delay) in the nervous system.[29]

[a]The *phase* is the initial angle of a sinusoidal component in a periodic signal, and it is specified in radians (or angular degrees). The phase difference between two signals indicates their relative timing, resulting from a dynamic relationship between them, e.g. a time delay.

To get a robust estimation of phase coupling, it is recommended to use phase synchrony (PS) measures such as phase coherence (also called phase locking value).[4,29,43,46–48] PS measures use the distribution of phase differences between signals (instead of the cross-spectrum) to quantify phase coupling, thus PS measures eliminate the impact of varying amplitude ratios.[43] A general notion of PS was first introduced to describe nonlinear phase coupling between any two frequencies, namely $n:m$ phase locking.[44] The resulting metric, namely $n:m$ synchronization index, quantifies the phase locking of n cycles of one oscillation to m cycles of another oscillation, where the two oscillations have a frequency ratio of m/n. Although the $n:m$ synchronization index can detect harmonic phase coupling, it is blind to the intermodulation phase coupling among multiple frequencies.[42] Many studies have indicated that intermodulation phase coupling might be linked to functional roles such as the integration of sensory information in the nervous system.[14,18,19,49]

The concept of PS has also been extended to quantify the second-order intermodulation phase coupling among three frequencies $\{f_1, f_2\} \to f_3$ (where $f_3 = f_1 + f_2$); the resulting metric is called bi-phase locking value (bPLV).[42] However, several studies have reported intermodulation beyond the second order in the visual system.[18,20,49] and in the sensorimotor system.[50,51] Thus, there is the potential interest of further extending the concept of PS to detect higher order ($>$2nd order) intermodulation phase coupling (e.g. $\{f_1, f_2\} \to 2f_2 - f_1, \{f_1, f_2, f_3\} \to f_3 + 2f_2 - f_1$). However, to the best of our knowledge, a mathematical description of this extension is still missing and real-world applications have not been shown in existing literature.

To fill this gap, we introduce the multi-spectral phase coherence (MSPC) as a general PS approach for quantifying any order intermodulation phase coupling, as well as harmonic phase coupling. Similar to existing PS measures, MSPC is based on the distribution of phase differences between signals. Because MSPC is independent of the signal's amplitude, it provides a more reliable quantification of nonlinear phase coupling and time delay between the two signals than high-order spectra measures. Distinct from existing PS measures, MSPC can access higher order intermodulation phase coupling, so as to provide a more complete description of nonlinear interactions in the nervous system. Additionally, MSPC is an asymmetric measure and therefore can indicate the directionality of interaction (i.e. the causality between signals). We demonstrate these features in a comparison between MSPC and two representative nonlinear PS measures, namely the $n:m$ synchronization index[44] (the measure for $n:m$ phase locking) and the bPLV[42] (the measure for QPC), in the analysis of simulated data.

To fully take advantage of MSPC, it is useful to define a set of basic frequencies and the expected relation between them, in terms of harmonic and intermodulation coupling. Periodic signals such as multi-sine, which is defined as the sum of multiple sinusoids, provide an excellent stimulus type to investigate nonlinear properties of a system by evoking the steady-state responses at the harmonic and intermodulation frequencies.[52] We applied the MSPC to analyze data recorded during a human motor control experiment. In this experiment, a multi-sine perturbation was imposed at the right wrist when the healthy subjects were instructed to keep an isotonic flexion with the same wrist by a visual feedback. We simultaneously recorded the perturbation signal, brain responses (EEG), and muscle activity (electromyogram, EMG); and then used MSPC to quantify the directional nonlinear connectivity between the periphery (the wrist perturbation and EMG) and the brain (EEG), as well as the time delay between the wrist perturbation and the brain response.

2. Phase Coupling and MSPC

In this section, first we provide the background of phase coupling, and introduce a generalized notion for any order nonlinear phase coupling among multiple frequencies. Then, we describe the proposed measure, MSPC, for quantifying different order nonlinear phase coupling as well as estimating the time delay between signals. In the end of this section, some practical issues for quantifying nonlinear interactions in the nervous system using MSPC are discussed.

2.1. *Phase coupling*

2.1.1. *Phase coupling between two frequencies*

Introduced by Huygens in 17th century, the classical notion of phase coupling (or phase synchronization) is typically defined as a locking of the phases at two frequencies between two time series (i.e. ideally the

phase difference is equal to a constant)[53]:

$$|\Delta\phi| = |n\phi(f_m) - m\phi(f_n)| = \text{const}, \quad (1)$$

where $\phi(f_m)$ and $\phi(f_n)$ are the phases of two time series at frequencies f_m and f_n, with the relation $nf_m = mf_n$, and $\Delta\phi$ the phase difference between them. This classical notion is known as $n:m$ phase locking,[44] which covers harmonic and iso-frequency coupling ($f_m = f_n$).

2.1.2. *Phase coupling between three frequencies*

In 1963, Hasselmann *et al.* introduced the QPC, a nonlinear phase coupling involving a pair of frequencies $\{f_1, f_2\}$ and the second-order intermodulation frequency ($f_3 = f_1 + f_2$).[30] QPC can be defined in a similar way as the classical phase coupling[42]:

$$|\Delta\phi| = |\phi(f_1) + \phi(f_2) - \phi(f_1 + f_2)| = \text{const}. \quad (2)$$

Typically, QPC can be shown in a simple second-order nonlinear system (e.g. $y = x^2$) when the input at least contains two frequencies.[40]

2.1.3. *Phase coupling among multiple frequencies and the generalized notion of nonlinear phase coupling*

Several studies have shown nonlinear phase coupling beyond the second order in the nervous system by detecting neural responses to periodic stimuli at higher order (>2) harmonic and intermodulation frequencies,[16,18–20,39,49–52] indicating the presence of higher order nonlinear interactions.

Consider a general case of a nonlinear system with a nonlinearity of the dth order, such as $y = x^d$. Using a multi-sine input signal with R different frequencies $f_1, f_2, \ldots, f_R (f_1 < f_2 < \cdots < f_R)$, the system can show the dth order nonlinear phase coupling between the set of input frequencies $\{f_1, f_2, \ldots, f_R\}$ and an output frequency,[54] which is a combination of the input frequencies, $f_\Sigma = \sum_{r=1}^{R} a_r f_r > 0 (a_r$ are integers, and $\sum_{r=1}^{R} |a_r| = d)$.

Thus, we introduce a generalized notion of high-order nonlinear phase coupling:

$$|\Delta\phi| = \left| \sum_{r=1}^{R} a_r \phi(f_r) - \phi(f_\Sigma) \right| = \text{const}. \quad (3)$$

This definition covers all possible harmonic and intermodulation coupling at any order of nonlinearity. For example, given a multi-sine input signal with three frequencies f_1, f_2, f_3 applied to a system with a third-order nonlinearity, e.g. $y = x^3$, then the output will include spectral components at the third-order harmonics, $3f_1, 3f_2$ and $3f_3$, and the third-order intermodulation frequencies, $f_3 \pm f_2 \pm f_1, 2f_r \pm f_l, f_r - 2f_l (r, l = 1, 2, 3, r \neq l)$, which are all nonlinearly phase coupled with the input frequencies as defined in Eq. (3).

2.2. *Multi-spectral phase coherence*

For the two time series $x(t)$ and $y(t)$ with K epochs,[b] $X(f)$ and $Y(f)$ are their Fourier transforms. The MSPC at the dth order is defined as the magnitude (denoted as ψ) of the complex measure called *multi-spectral phase coherency* (denoted as Ψ): $\psi = |\Psi|$, for quantifying dth nonlinear phase coupling (including both harmonic and intermodulation coupling). The multi-spectral phase coherency Ψ is defined by:

$$\Psi_{XY}(f_1, f_2, \ldots, f_R; a_1, a_2, \ldots, a_R)_d = \frac{1}{K} \sum_{k=1}^{K} \exp\left(j \left(\sum_{r=1}^{R} a_r \phi_{X_k}(f_r) - \phi_{Y_k}(f_\Sigma) \right) \right), \quad (4)$$

where f_Σ is an output frequency of $Y(f)$ as defined before, $f_1, f_2, \ldots, f_R$ are the input frequencies of $\mathrm{X}(f)$, $\phi_{X_k}(f_r)$ is the phase of $X(f_r)$ at kth epoch, $a_1, a_2, \ldots, a_R$ are the weights of input frequencies to corresponding output frequency f_Σ and $\sum_{r=1}^{R} |a_r| = d$. Details about computation of MSPC are given in Appendix A.

As the magnitude of Ψ_{XY}, MSPC (ψ_{XY}) reflects the consistency of nonlinear cross-frequency phase difference over epochs. Similar to other PS measures, MSPC reflects the "pure" phase relationship between two signals, independently of the signal's amplitude. The value of MSPC varies between 0 and 1, where 1 indicates that the nonlinear phase relationship is perfectly consistent across epochs, and 0 indicates that

[b] An *epoch* is a segment of a signal, relative to a stimulus event. In this work, "epoch" refers to a segment of data recorded during one period ($T = 1$s) of the stimulation signal.

the nonlinear phase relationship is completely random. For a total number of epochs K, the 95% significance threshold of MSPC equals $\sqrt{3/K}$, as indicated by a Monte Carlo simulation (see Appendix B). By computing different order MSPC, we can detect the harmonic and intermodulation coupling at different orders by checking the significance of MSPC values, so as to determine the order of nonlinearity in a system.

MSPC can also indicate the direction of interaction. Unless the relationship between two signals is linear, MSPC is an asymmetric measure: $\psi_{XY} \neq \psi_{YX}$, where ψ_{XY} indicates if the phase of frequency f_Σ in signal Y depends on the phases of the input frequencies $f_1, f_2, \ldots, f_R$ in signal X. In other words, ψ_{XY} quantifies the contribution of $\{\phi_X(f_r)\}_R$ in predicting $\phi_Y(f_\Sigma)$. If there is a time delay (nonzero phase lag) between the two signals, then ψ_{XY} can be used to indicate nonlinear Granger causality.[55] To underline its directionality, ψ_{XY} can also be denoted as $\psi_{X\to Y}$.

2.3. *Time delay estimation*

Assume that $x(t)$ leads $y(t)$ with a time delay $\tau > 0$ (standard unit: "second"), there is a phase lag between $X(f)$ and $Y(f)$: $\Delta\phi_{XY} = 2\pi f_\Sigma \tau$. Phase lag information can be extracted either by the expression $\arctan(\mathrm{Im}(\Psi_{XY})/\mathrm{Re}(\Psi_{XY}))$ or $\exp(j\Delta\phi_{XY}) = \Psi_{XY}/\psi_{XY}$. The former expression can directly get the phase value; however, this value is the modulus of the division of the true phase lag by 2π, which is known as *wrap-around effect*.[56] To avoid the wrap-around effect, we use the latter expression to estimate the time delay:

$$\tau_{\mathrm{est}} = \min_{\tau} \left(\sum_{f_\Sigma = \sum_{r=1}^{R} a_r f_r} \left| \exp(j(2\pi f_\Sigma \tau)) - \frac{\Psi_{XY}(f_1, f_2, \ldots f_R, a_1, a_2, \ldots, a_R)}{\psi_{XY}(f_1, f_2, \ldots f_R, a_1, a_2, \ldots, a_R)} \right| \right). \quad (5)$$

To verify the estimated time delay τ_{est}, one can perform a linear regression using least squares on the estimated phase values over frequencies (f_Σ) to get the confidence interval of the phase–frequency slope. Note that the number of cycles contained in $\Delta\phi_{XY}$ can be obtained according to $p = \mathrm{floor}(f_\Sigma \cdot \tau_{\mathrm{est}})$, so as to get the estimated phase lag for each frequency combination by:

$$\Delta\phi_{XY}^{(\mathrm{est})} = \arctan(\mathrm{Im}(\Psi_{XY})/\mathrm{Re}(\Psi_{XY})) + 2p\pi. \quad (6)$$

2.4. *Practical issues for identifying nonlinear interactions using MSPC*

A practical paradigm to investigate nonlinear interactions in the nervous system is the analysis of nonlinear phase coupling of the steady-state neural response to a periodic stimulus.[57] To fully exploit the advantage of MSPC, we suggest to use a multi-sine signal as the periodic stimulus, since it can elicit a rich class of nonlinear interactions including both harmonic and intermodulation coupling,[52,58] which is otherwise impossible to generate by using only a sinusoid stimulus.

Proper choice of the excited frequencies in the multi-sine stimulus allows for easy visualization of MSPC values. In the general case, MSPC is a function of $2 \times R$ variables (R frequency variables and R weight variables), which causes difficulties in visually representing MSPC when R is larger than 2. In practice, given either the known input frequencies or the weights, the dimensionality of variable space can be reduced to R. For example, the QPC can be described by the second-order MSPC with $a_1 = a_2 = 1$, which has only a 2D variable space. In this case, MSPC values for different frequency combinations can be plotted in a 2D map over two frequencies. Given an ideal set of input frequencies, the MSPC values can be plotted as a spectrum of the output frequency if there is no overlap of the given combinations of input frequencies. Noteworthy, the overlap of the output frequency for different input frequency combinations does not cause ambiguous estimation of nonlinear phase coupling as measured by MSPC, because the phase dependence of the output frequency f_Σ on different combinations are not the same.[52] Nonetheless, it is preferred to design a multi-sine stimulus containing frequencies such that overlapping of harmonic and intermodulation frequencies is minimized within the frequency range of the system's response. It is worth to note that nervous system responses usually have a limited frequency range due to their intrinsic properties. A practical rule for design of multi-sine stimulus is to only include frequencies that are ratios between

Table 1. Harmonic and intermodulation frequencies of 7, 13 and 29 Hz.

Order	Type of nonlinearity	Frequency combinations ($r, l = 1, 2, 3, r \neq l$)	Output frequency f_Σ (Hz)
2	Harmonics	$2f_r$	14, 26, 58
	Intermodulation	$f_r \pm f_l > 0$	6, 16, 20, 22, 36, 42
3	Harmonics	$3f_r$	21, 39, 87
	Intermodulation	$2f_r \pm f_l > 0$	1, 19, 27, 33, 43, 45, 51, 55, 65, 71
		$f_r - 2f_l > 0$	3, 15
		$f_3 \pm f_2 \pm f_1 > 0$	9, 23, 35, 49

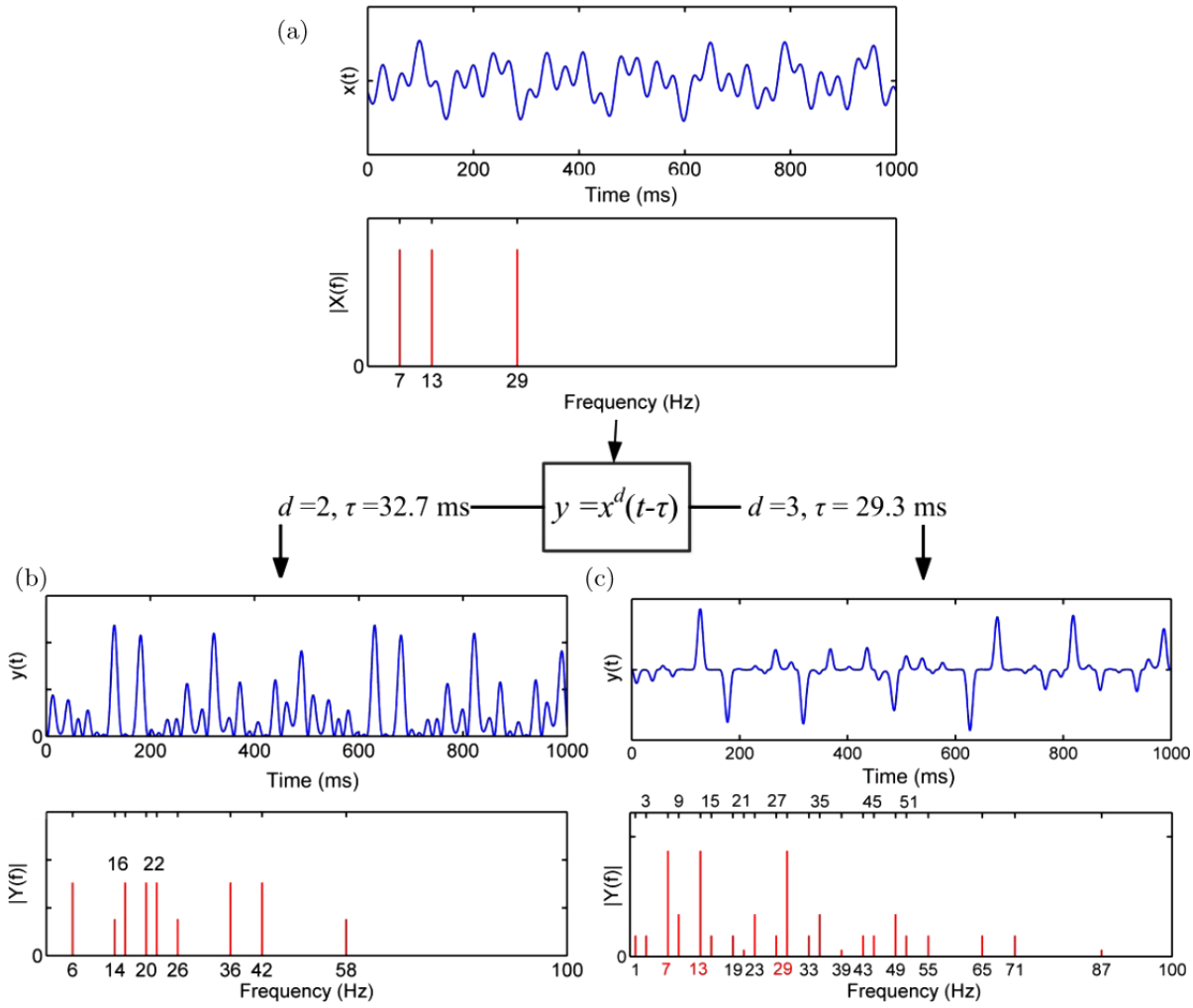

Fig. 2. (Color online) Simulated nonlinear systems. (a) Input signal: a multi-sine signal (period: 1 s, 600 epochs, sampling rate: 2048 Hz) with three frequency components at 7, 13, 29 Hz. Blue curve shows a single epoch of signal in the time domain, red lines indicate its amplitude spectrum. (b) Output signal from the second-order nonlinear system. The output signal contains frequency components at the second-order harmonic and intermodulation frequencies. (c) Output signal from the third-order nonlinear system. This output contains frequency components at the third-order harmonic and intermodulation frequencies.

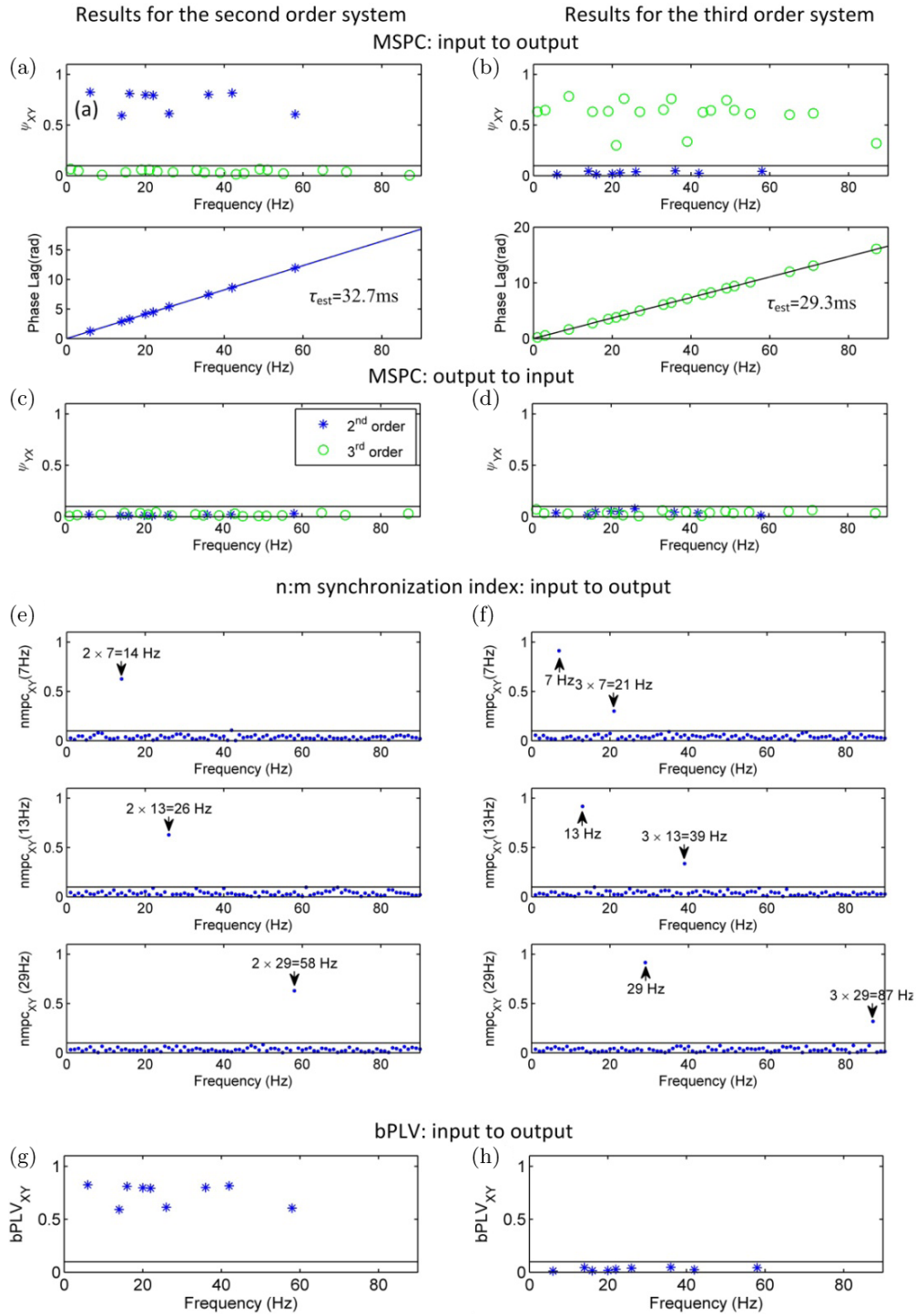

Fig. 3. (Color online) Simulation results. Top section (a–d): MSPC, time delay and phase lag estimation. In this section, blue stars indicate the second-order nonlinear interactions, green circles represent the third-order nonlinear interactions. (a) and (b) MSPC from input to output for the second-order and third-order nonlinear systems, respectively. (c) and (d) MSPC from output to input. Middle section (e and f): Harmonic relations between input and output as determined by $n:m$ phase synchronization index for the second-order (e) and third-order (f) nonlinear systems. Bottom section (g and h): Second-order phase coupling as determined by bPLV for the second-order (g) and third-order (h) nonlinear systems. All results are plotted as a function of f_{Σ}, since there is no overlap in the output frequencies. The horizontal line indicates the 95% confidence threshold.

odd prime integers and the period of signal, selecting those frequencies that minimize the overlap.

3. Simulations

To verify the effectiveness of MSPC, we simulated nonlinear systems and compared MSPC with two representative nonlinear PS measures, i.e. $n:m$ synchronization index[44] and bPLV.[42]

3.1. *Nonlinear systems and parameter selection*

We simulated nonlinear systems with the output–input relationship: $y = x^d(t - \tau)$. Without loss of generality, MSPC was tested with a second-order and third-order nonlinear systems with two arbitrary time delays, i.e. $\tau = 32.7$ ms for the second order and $\tau = 29.3$ ms for the third-order system. The system input was a multi-sine signal (period: 1 s) consisting of three sinusoids of 7, 13, 29 Hz with randomly chosen phases. The input frequencies were chosen to avoid any overlap in the second-order and third-order harmonic and intermodulation frequencies (see Table 1), so the origin of the frequency components in the output can be easily separated and MSPC values can be plotted as a spectrum of the output frequency.

The systems were simulated for 600 s at a sample rate of 2048 Hz. Figure 2 shows one period of the input and output signals and their amplitude spectra. The second-order system generated frequency components in the second-order harmonic $2f_r$ and the intermodulation frequencies $f_r \pm f_l (r, l = 1, 2, 3, r \neq l)$, while the third-order system yielded frequency components in the third-order harmonics $3f_r$ and intermodulation frequencies $f_3 \pm f_2 \pm f_1, 2f_r \pm f_l, f_r - 2f_l$, as well as in the fundamental frequencies. Before calculating MSPC and other PS measures, independent white noise signals were added to the input and output signals (SNR $= -20$ dB). To keep consistency with existing literature, the value of SNR were given in time domain and expressed in the logarithmic decibel scale. We used MATLAB function (awgn.m) to add the noise.

3.2. *Advantages of MSPC over other measures*

The second-order and third-order MSPC, $n:m$ synchronization index[44] and bPLV[42] were computed between the input and the output. The results of these analyses are shown in Fig. 3. for comparison. We used a 95% confidence threshold ($\alpha = 0.05$) to determine the significance of phase coupling. The MSPC values from input to output are significant at the harmonics and intermodulations with the same order as the corresponding nonlinear system; while, as expected, the MSPC from output to input shows no significant values. Using Eq. (5), we correctly estimated the time delay of the nonlinear systems. The $n:m$ synchronization index only detected iso-frequency and harmonic phase coupling, and failed to identify any intermodulation coupling. The bPLV was only capable to detect second-order nonlinear interactions.

Overall, the simulation showed that MSPC can detect different order harmonic and intermodulation coupling, correctly indicate the direction of nonlinear interaction, and precisely estimate the time delay in nonlinear systems. Additionally, we also investigated the robustness of MSPC to the level of noise (see Appendix C). MSPC can reliably detect nonlinear interactions and precisely estimate the time delay in the system as long as the signal-to-noise ratio (SNR) is higher than -35 dB. This indicates that MSPC should be suitable for detecting the nonlinear phase coupling between neurophysiological signals, such as EEG and EMG, since scalp EEG has a SNR typically between -6 and -32 dB,[59] and surface EMG has a SNR typically between -5 and -15 dB.[60]

4. Application: Nonlinear Connectivity in the Sensorimotor System

4.1. *Experiment and data recording*

Eleven healthy right-handed subjects (age between 20 and 29, four women) participated in a motor control experiment. All subjects gave written informed consent prior to their participation. The experimental procedure was approved by the Human Research Ethics Committee of the Delft University of Technology.

In the experiment, the subjects were instructed to exert a constant flexion torque (1 Nm) with their right wrist, while a robotic wrist manipulator (Wristalyzer, Moog Inc., the Netherlands) applied a periodic movement as a perturbation (period: 1 s, peak-to-peak amplitude: 0.06 rad). The perturbation signal was a multi-sine with three frequencies, i.e. 7,

13 and 29 Hz and randomly chosen phases. We used this multi-sine perturbation as an external input to probe the nonlinearity in the sensorimotor system. Previous studies showed that periodic somatosensory stimuli typically evoke nonlinear responses in the second and third order.[51,61] The three frequencies in the multi-sine allow to study the second- and third-order nonlinear interactions in the sensorimotor system without overlap in the harmonic and intermodulation frequencies (see also Table 1). In this case, we can easily test the hypothesis that MSPC can effectively quantify nonlinear connectivity in the human sensorimotor system, in term of the second- and third-order nonlinearities. Each subject performed 60 trials of 22 s each, with 1 s fade-in and 1 s fade-out periods.

The EEG was recorded using a 128-channel cap (according to the 5–10 systems, WaveGuard cap, ANT Neuro) with Ag/AgCl electrodes. The EMG was recorded from the flexor carpi radialis muscles (EMGflex) and the extensor carpi radialis muscles (EMGext) using bipolar derivations (two Ag/AgCl electrodes, center-to-center distance: 2 cm). All neurophysiological (EEG and EMG) and mechanical signals (wrist angle and wrist torque) were digitized at 2048 Hz and stored for offline analyses (Refa System, TMSi, Oldenzaal, the Netherlands).

4.2. *Data processing*

To remove the fade-in/out and other transient responses, the first 3 s and the last 2 s of each trial were excluded from data analysis. The data were segmented into consecutive nonoverlapping 1-s epochs, giving a total of $60 \times (22-3-2) = 1020$ epochs. The EEG data were visually inspected. Epochs contaminated by artifacts (e.g. eye blinking and saccades) and channels with excessive noise were removed. Table 2 indicates the number of epochs removed for analysis, as well as the number of electrodes rejected. After artefact removal, we obtained more than 720 epochs for each subject. This amount of epochs has been shown to be sufficient (> 360 epochs) for a reliable nonlinear analysis on EEG.[62] Most of the rejected channels were located on the periphery of the montage, where EMG artifacts are expected. After artifact removal, the EEG was referenced to the common average. To remove the power-line (50 Hz) and possible movement artifacts,

Table 2. Number of rejected and retained epochs and channels.

	Epochs (1020 in total[a])		EEG channels (128 in total)	
Subject	Removed	Rest	Removed	Rest
01	96	924	12	116
02	172	848	10	118
03	72	948	3	125
04	77	943	6	112
05	291	729	0	128
06	81	939	17	111
07	20	1000	0	128
08	225	795	21	107
09	52	968	8	120
10	225	795	7	121
11	39	777	13	105

[a]Subject 11 only has 816 epochs in total, since he only performed 48 trials due to limited availability.

notch and bandpass filtering was applied to the EMG[60]: the EMG were transformed to the frequency domain using the Fourier transform; frequency components at 50 Hz and below 35 Hz (as well as the mirror part on the right side of spectrum) were set to zero and the EMG was transformed back to the time domain by inverse Fourier transform. As the movement perturbation contains frequency components at 7, 13 and 29 Hz, the cut-off frequency of the high-pass filtering was chosen to ensure that no movement artifacts are included in the analysis. Subsequently, the filtered EMG were rectified to extract the grouped motor unit (MU) activities by shifting the peak of the MU action potential spectrum toward the lower firing rate frequencies, which results in the low frequency components of the filtered and rectified EMG (for details, see Ref. 73).

MSPC between the multi-sine perturbation signal and the EEG (denoted as $\psi_{P\to\mathrm{EEG}}$) was calculated for the second-order and third-order nonlinearities, to quantify nonlinear connectivity from the stimulus to the cortical response, as well as the time delay $\tau_{P\to\mathrm{EEG}}$. The time delay was estimated using only the output frequencies with significant MSPC. For visualization, the scalp distribution of $\psi_{P\to\mathrm{EEG}}$ was obtained by calculating the average MSPC over the frequency combinations for each EEG channel. The results of $\psi_{P\to\mathrm{EEG}}$ and time delay were presented in the EEG channel with

the highest average MSPC for each subject. To explore nonlinear cortico-muscular connections and their directionality, we also computed $\psi_{\mathrm{EEG}\to\mathrm{EMG}}$ and $\psi_{\mathrm{EMG}\to\mathrm{EEG}}$ between EEG and EMGflex at the same frequency combinations as those for $\psi_{P\to\mathrm{EEG}}$.

4.3. *Results*

4.3.1. *Nonlinear brain response to multi-sine stimulus*

Figure 4 shows the result of $\psi_{P\to\mathrm{EEG}}$ for a representative subject. Both the second-order and third-order harmonic and intermodulation coupling between EEG and the perturbation were detected. For this subject, the estimated time delay $\tau_{P\to\mathrm{EEG}}$ was 40.4 ms. The time delay $\tau_{P\to\mathrm{EEG}}$ (solid line in Fig. 4(b)) matches with the distribution of phase values for individual output frequencies (within the 95% confidence interval of phase–frequency slope), indicating that it is reasonable to assume that there is only one time delay, possibly shared by the different order nonlinear interactions. The scalp topography of the average $\psi_{P\to\mathrm{EEG}}$ is shown in Fig. 4(c). The large mean values (red area) are shown in the electrodes on the left hemisphere (contralateral to the stimulation), near the somatosensory cortex.

The group level results are shown in Fig. 5. All subjects showed significant second- and third-order MSPC values. The average time delay $\tau_{P\to\mathrm{EEG}}$ over subjects was 43 ± 8 ms (mean $\pm$ std.). The average scalp topography of $\psi_{P\to\mathrm{EEG}}$ (Fig. 5(b)) is similar to the example in Fig. 4(c), and the peak value is localized at electrode CCP3h, approximately over the left somatosensory cortex.

4.3.2. *Directional interactions between brain and muscle in the perturbed motor control*

The results of $\psi_{\mathrm{EEG}\to\mathrm{EMG}}$ and $\psi_{\mathrm{EMG}\to\mathrm{EEG}}$ for the same representative subject are shown in Fig. 6. The

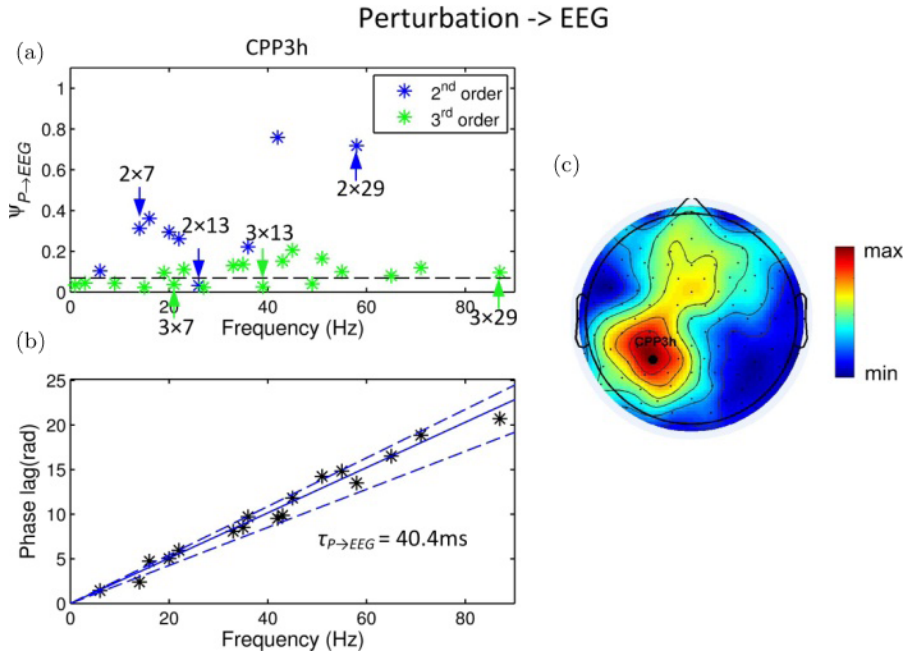

Fig. 4. (Color online) Nonlinear interaction between the perturbation and EEG signals for a representative subject. (a) Second-order and third-order MSPC ($\psi_{P\to\mathrm{EEG}}$). The result is shown for channel CPP3h, which has the largest mean significant $\psi_{P\to\mathrm{EEG}}$. The horizontal line indicates the 95% confidence threshold. The MSPC values for harmonic coupling are pointed out by arrows. All other values correspond to intermodulation coupling. (b) Estimated nonlinear phase lag. The solid line was generated from the estimated time delay $\tau_{P\to\mathrm{EEG}} = 40.4$ ms. Only phase lags with significant MSPC values are shown. The dashed lines indicate the 95% confidence interval of phase–frequency slope fitted to the phase lags by least squares. Our estimated time delay lies inside the confidence interval, which validates the result of our time delay estimation. (c) Scalp topography of the mean significant $\psi_{P\to\mathrm{EEG}}$. Only the electrodes on the scalp are shown. Black dots indicate the electrode positions. The electrode with the peak value is marked out by a filled circle.

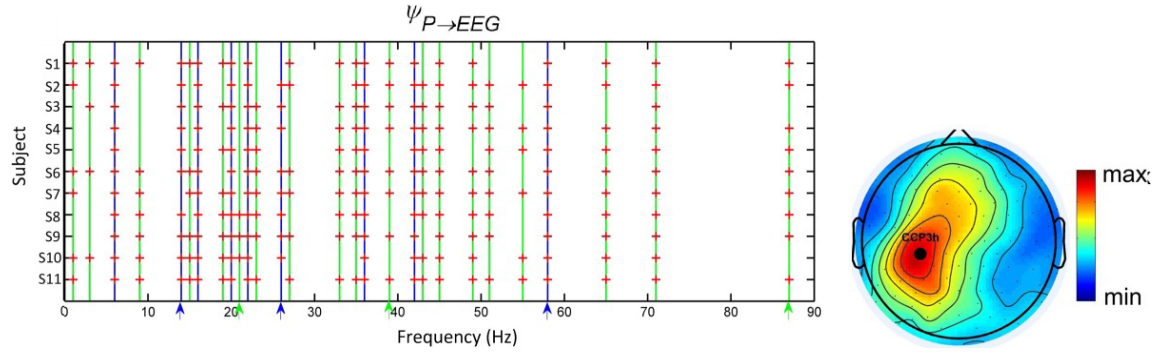

(a) (b)

Fig. 5. (Color online) Significant MSPC between the perturbation and EEG signals across subjects. (a) Overview of significant MSPC for all subjects. Vertical lines indicate the second-order (blue) and third-order (green) nonlinear interactions. The harmonics and intermodulations with significant MSPC are marked with red crosses. (b) Grand average of normalized topography of MSPC magnitude over the subjects. We normalized the MSPC values in each electrode by dividing over the maximum for each subject before computing the grand average, so as to equalize the contribution of each subject. Only the electrodes on the scalp are shown. Black dots indicate the electrode positions, and the electrode with the peak value is marked out by a solid circle.

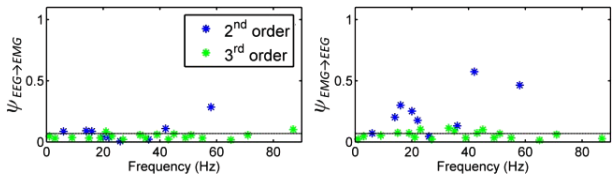

Fig. 6. Nonlinear connectivity in the efferent ($\psi_{\mathrm{EEG}\to\mathrm{EMG}}$) and afferent ($\psi_{\mathrm{EMG}\to\mathrm{EEG}}$) pathways for one representative subject. The horizontal line indicates the 95% confidence threshold. Significant MSPC occurs more often in $\psi_{\mathrm{EMG}\to\mathrm{EEG}}$ than $\psi_{\mathrm{EEG}\to\mathrm{EMG}}$ with larger magnitudes.

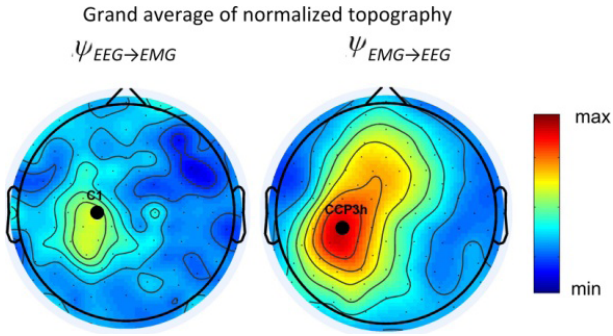

Fig. 7. Grand average of normalized topographies of $\psi_{\mathrm{EEG}\to\mathrm{EMG}}$ and $\psi_{\mathrm{EMG}\to\mathrm{EEG}}$. Only the electrodes on the scalp are shown. Black dots indicate the electrode positions, and the electrode with the peak value is marked with a filled circle in each plot.

efferent ($\mathrm{EEG}\to\mathrm{EMG}$) and afferent ($\mathrm{EMG}\to\mathrm{EEG}$) pathways have significant MSPC occurring at different frequency combinations and with different magnitudes. Noteworthy, the nonlinear interactions are stronger for the second-order relationships and the afferent pathway, with minimal amplitude of MSPC in the efferent pathway. Similar results are present in all subjects. The differences between $\psi_{\mathrm{EEG}\to\mathrm{EMG}}$ and $\psi_{\mathrm{EMG}\to\mathrm{EEG}}$ are also shown in their scalp distributions (see Fig. 7). The averaged topography of $\psi_{\mathrm{EMG}\to\mathrm{EEG}}$ is similar to that of $\psi_{P\to\mathrm{EEG}}$ (compare Fig. 7 to Fig. 5(b)) with the peak value at the same electrode CCP3h (near the somatosensory cortex); whereas the peak value of $\psi_{\mathrm{EEG}\to\mathrm{EMG}}$ is located at electrode position C1, which is closer to the motor cortex.

5. Discussion and Conclusions

We introduced a novel approach to quantify directional nonlinear connectivity in the nervous system. By filling the gap of assessing higher order intermodulation coupling, MSPC provides a general tool for measuring the amplitude-independent nonlinear phase coupling. The advantages of MSPC over existing phase coupling measures become evident when a multi-sine stimulus is presented as an input to the nervous system. Applying MSPC to data recorded during a motor control experiment, we revealed directional nonlinear connectivity between the periphery (the somatosensory stimulus

and muscular activity) and the central nervous system (the brain activity); as well as the time delay in the afferent pathway from the periphery to the brain.

5.1. *Comparison with existing PS measures*

MSPC quantifies the amplitude-independent nonlinear phase coupling including different order harmonic and intermodulation coupling. MSPC can be considered as an extension of amplitude-independent QPC measures (e.g. bPLV), which incorporates higher-order nonlinearities. Thus it presents a more complete description of the nonlinear phase interactions. In contrast to the $n:m$ phase locking measures,[44,63] which typically refer to the phase locking between two different frequencies, MSPC describes the case where a group of fundamental frequencies is coupled to one frequency (group-to-one coupling), which is a combination of the fundamental frequencies. Although the $n:m$ phase locking can be extended to a multivariate case using pairwise strategy,[64] this extension still describes a collection of phase locking values between frequency pairs instead of the group-to-one coupling. Hence, the $n:m$ phase locking measure can never detect the intermodulation coupling whereas MSPC does.

5.2. *Nonlinear connectivity and time delay*

Neural interactions are commonly referred to as functional connectivity or effective connectivity. Functional connectivity reflects neural correlation without directionality, while effective connectivity represents an asymmetric or causal dependency between neural activities.[65,66] In the nervous system, functional and effective connectivity include linear and nonlinear processes. Iso-frequency phase coupling measures are often used to assess linear functional connectivity.[29] As a complement to linear measures, MSPC provides a general tool to detect nonlinear connectivity by quantifying phase coupling across frequencies and to indicate the order of nonlinearity. Furthermore, the asymmetry of MSPC allows for the detection of directional dependency between signals. Being a model-free method, MSPC presents an alternative tool to estimate the potential effective connectivity without prior knowledge of a model structure.

Effective connectivity in the nervous system is usually associated with a time delay, which is physiologically meaningful. For frequency domain methods, the time delay can be estimated through the phase lag between signals.[67] Previous studies often utilized the inverse tangent of the ratio between the imaginary part and the real part of the cross-spectrum (or high-order spectra) to estimate the phase lag.[37,56,68] We provide an alternative way to estimate the time delay using the MSPC (see Eq. (5)), which is able to overcome the warp-around effect in phase lag estimation and to reduce the potential bias from nonstationary amplitude ratio between signals.

5.3. *Applications: Nonlinear connectivity in motor control*

We used MSPC to quantify the nonlinear connectivity from the periphery to the brain and from the brain to the muscle, in a perturbed isotonic wrist flexion task. The participants in our experiment tried to keep a constant flexion torque while receiving a multi-sine perturbation; a challenging task for the motor control system.

Results of MSPC demonstrate harmonic and intermodulation interactions between the multi-sine perturbation and the brain responses. These results are in line with previous findings of nonlinear steady-state responses to periodic somatosensory stimuli.[50,51,61] The scalp topography of $\psi_{P\rightarrow \mathrm{EEG}}$ is also very similar to the topographies previously shown in somatosensory steady-state evoked responses.[50,51,57] Our results suggest the effectiveness of MSPC on detecting and mapping the nonlinear connectivity from a periodic stimulus to the brain.

Previous studies.[17,50,51,61] detected the presence of nonlinear interactions between a periodic stimulus with one or two frequency components and the brain response, by comparing the amplitude spectrum or phase resetting (inter-trial coherence.[69,70]) of the EEG response and background EEG activity; without any indication of a time delay in the response. MSPC provides a direct way to quantify the nonlinear stimulus-to-brain connectivity through phase coupling, and to estimate the time delay. Using a multi-sine stimulus takes the full advantage of MSPC, since (1) multi-sine stimulus can elicit more harmonic and intermodulation coupling than

single- or bi-frequency stimulus; and (2) therefore more frequencies can be used to have a better estimation of time delay.

The time course of the cortical responses to a peripheral stimulus is typically studied by event-related potential (ERP)[71] evoked by a transient events, particularly by the latency of its components (positive and negative peaks). Using ERPs, the first dominant scalp EEG response to transient mechanical stimulation of the finger/hand is known as P45/P50, a positive deflection occurring between 40 and 50 ms after the stimulus onset.[51,72] The source of the P45/P50 response is located the primary somatosensory cortex.[72] Nevertheless, when using a multi-sine perturbation, one cannot estimate the time delay from the latency of ERP components anymore due to the continuous stimulus. Instead, we used MSPC to estimate the time delay between the perturbation and EEG signals. Our estimated time delay is 43 ± 8 ms, which is in line with the previous findings from analyzing ERPs after transient mechanical stimulation of the finger/hand. Furthermore, the channel with the largest MSPC values was consistently located around the primary somatosensory area.

We also used MSPC to explore the corticomuscular connectivity. For several decades, corticomuscular connectivity has been investigated by linear coherence between EEG and EMG, known as corticomuscular coherence (CMC).[73] Since CMC is a linear method, it is blind to nonlinear interactions.[74] and cannot separate the interactions in the efferent ($\mathrm{EEG} \rightarrow \mathrm{EMG}$) and afferent ($\mathrm{EMG} \rightarrow \mathrm{EEG}$) pathways.[56] To eliminate the ambiguity of CMC, some researches employed linear causality measures such as partial directed coherence and directional transfer function to separate these two pathways.[56,75] However, these methods are still limited in quantifying linear connectivity between the two signals. MSPC probes the nonlinear cortico-muscular connection. We quantified the nonlinear connectivity from EEG to EMG (efferent pathway) and from EMG to EEG (afferent pathway) during a force generation task with a mechanical perturbation. We found different behavior between $\psi_{\mathrm{EEG} \rightarrow \mathrm{EMG}}$ and $\psi_{\mathrm{EMG} \rightarrow \mathrm{EEG}}$, further indicating that corticomuscular interaction is nonlinear, since a pure linear interaction should generate the same results for $\psi_{\mathrm{EEG} \rightarrow \mathrm{EMG}}$ and $\psi_{\mathrm{EMG} \rightarrow \mathrm{EEG}}$.

In our analysis, $\psi_{\mathrm{EMG} \rightarrow \mathrm{EEG}}$ and $\psi_{P \rightarrow \mathrm{EEG}}$ reflect nonlinear connectivity in the afferent pathway of motor control, whereas $\psi_{\mathrm{EEG} \rightarrow \mathrm{EMG}}$ indicates nonlinear connectivity in the efferent pathway. Accordingly, we found similar scalp distributions of $\psi_{\mathrm{EMG} \rightarrow \mathrm{EEG}}$ and $\psi_{P \rightarrow \mathrm{EEG}}$, different from $\psi_{\mathrm{EEG} \rightarrow \mathrm{EMG}}$. Moreover, the electrode with the largest MSPC differs between afferent (electrode position: CCP3h) and efferent (electrode position: C1) pathways, in agreement with the more posterior location of primary somatosensory cortex as compared to primary motor cortex.

5.4. *Potential applications*

In this work, we demonstrate the application of MSPC in quantifying nonlinear connectivity between the periphery and the brain using an external stimulus. However, MSPC can also be applied without the need of stimuli. Similar to other PS measures, MSPC can be used to detect phase coupling between two or more signals with broad frequency spectra by scanning possible frequency combinations based on an expected relation. For example, if the expected relation between two signals X and Y is $\{f_r, f_l\} \rightarrow f_\Sigma = 2f_r - f_l$, MSPC can be computed between any arbitrary frequency pair $\{f_r, f_l\}$ in X and their corresponding intermodulation frequency $f_\Sigma = 2f_r - f_l$ in Y. False positives resulting from pure linear interactions can be excluded by checking the asymmetry of MSPC ($\psi_{XY} \neq \psi_{YX}$). Thus MSPC could also be useful for detecting nonlinear connectivity between different brain areas.

Acknowledgments

The research leading to these results has received funding from the European Research Council under the European Union's Seventh Framework Programme (FP/2007–2013)/ERC Grant Agreement No. 291339 (4D-EEG project). Alfred C. Schouten and Frans C. T. Van der Helm contributed equally.

Appendix A. Details of MSPC Computation

The MSPC ψ_{XY} is defined as the magnitude of the *multi-spectral phase coherency* Ψ_{XY}, which is given between two frequency domain signals $X(f)$ and

$Y(f)$ as:

$$\Psi_{XY}(f_1, f_2, \ldots, f_R; a_1, a_2, \ldots, a_R)_d = \frac{1}{K}\sum_{k=1}^{K}\exp\left(j\left(\sum_{r=1}^{R} a_r\phi_{X_k}(f_r) - \phi_{Y_k}(f_\Sigma)\right)\right), \tag{A.1}$$

where K is the total number of epochs, $f_1, f_2, \ldots, f_R$ are the input frequencies in $\mathrm{X}(f)$, $a_1, a_2, \ldots, a_R$ are the weights of the input frequencies to the output frequency $f_\Sigma = \sum_{r=1}^{R} a_r f_r > 0$, with a_r integer numbers, d is the order of the nonlinearity ($\sum_{r=1}^{R}|a_r| = d$).

Note the expression: $\exp(z_1 + z_2) = \exp(z_1)\cdot\exp(z_2)$, where z_1, z_2 can be complex numbers. If $a_r \geq 0 (r = 1, \ldots, R)$, then Eq. (A.1) can be written as:

$$\Psi_{XY}(f_1, f_2, \ldots, f_R; a_1, a_2, \ldots, a_R)_d = \frac{1}{K}\sum_{k=1}^{K}\left(\prod_{r=1}^{R}(\exp(j\phi_{X_k}(f_r)))^{a_r} \cdot \exp(-j\phi_{Y_k}(f_\Sigma))\right). \tag{A.2}$$

Since $X_k(f_r) = |X_k(f_r)|\exp(j\phi_{X_k}(f_r))$ and $Y^*(f_\Sigma) = |Y(f_\Sigma)|\exp(-j\phi(f_\Sigma))$ (the symbol '$*$' indicates complex conjugate), Ψ_{XY} can be computed by:

$$\Psi_{XY}(f_1, f_2, \ldots, f_R; a_1, a_2, \ldots, a_R)_d = \frac{1}{K}\sum_{k=1}^{K}\left(\prod_{r=1}^{R}\frac{X_k^{a_r}(f_r)}{|X_k(f_r)|^{a_r}}\cdot\frac{Y_k^*(f_\Sigma)}{|Y_k(f_\Sigma)|}\right), \tag{A.3}$$

where $X_K^0(f_r) = 1$ and $X_k^{a_r}(f_r) = \underbrace{X_k(f_r)X_k(f_r)\cdots X_k(f_r)}_{a_r}$.

If $\{a_r\} = \{a_s, a_l\}$, where $a_s \geq 0$ and $a_l < 0 (s \neq l, s, l \in \{1, \ldots, R\})$, then Eq. (A.1) can be written as:

$$\Psi_{XY}(f_1, f_2, \ldots, f_R; a_1, a_2, \ldots, a_R)_d = \frac{1}{K}\sum_{k=1}^{K}\exp\left(j\left(\sum_{s} a_s\phi_{X_k}(f_s) - \sum_{l}|a_l|\phi_{X_k}(f_l) - \phi_{Y_k}(f_\Sigma)\right)\right). \tag{A.4}$$

In this case, Ψ_{XY} can be computed by:

$$\Psi_{XY}(f_1, f_2, \ldots, f_R; a_1, a_2, \ldots, a_R)_d = \frac{1}{K}\sum_{k=1}^{K}\left(\prod_{s}\frac{X_k^{a_s}(f_s)}{|X_k(f_s)|^{a_s}} \cdot \prod_{l}\frac{(X_k^*(f_l))^{|a_l|}}{|X_k(f_l)|^{|a_l|}}\cdot\frac{Y_k^*(f_\Sigma)}{|Y_k(f_\Sigma)|}\right). \tag{A.5}$$

Although in this paper MSPC is defined in the frequency domain, it is noteworthy that the concept of MSPC can be extended to the time–frequency domain to detect and quantify the instantaneous nonlinear phase coupling between two signals by computing the *time-dependent* multi-spectral phase coherency and taking its magnitude:

$$\Psi_{XY}(f_1, f_2, \ldots, f_R; a_1, a_2, \ldots, a_R; t)_d = \frac{1}{K}\sum_{k=1}^{K}\exp\left(j\left(\sum_{r=1}^{R} a_r\phi_{X_k}(f_r, t) - \phi_{Y_k}(f_\Sigma, t)\right)\right). \tag{A.6}$$

Instantaneous phases of signals at different frequencies can be obtained by either Gabor wavelet or Hilbert transform (see Refs. 43 and 76 for details and 24 for a review).

Appendix B. Significance Level of MSPC

Let $\Delta\phi_{XY}^{(k)}$ be the cross-frequency phase difference between signals for a given frequency combination: $\Delta\phi_{XY}^{(k)} = \sum_{r=1}^{R} a_r\phi_{X_k}(f_r) - \phi_{Y_k}(f_\Sigma)$, then MSPC ($\psi_{XY}$) is given as:

$$\psi_{XY} = \left|\frac{1}{K}\sum_{k=1}^{K}\exp(j\Delta\phi_{XY}^{(k)})\right| = \left|\frac{1}{K}\sum_{k=1}^{K}\exp(j\tilde{\Delta}\phi_{XY}^{(k)})\right|, \tag{B.1}$$

where $\tilde{\Delta}\phi_{XY}^{(k)} \equiv \Delta\phi_{XY}^{(k)} \bmod 2\pi$. The null hypothesis is that $\Delta\phi_{XY}^{(k)}$ is completely random so that $\tilde{\Delta}\phi_{XY}^{(k)}$ will be uniformly and randomly distributed in the interval $[0, 2\pi]$. Shils analytically determined the theoretical 95% confidence threshold of $|\sum_{k=1}^{K}\exp(j\phi^{(k)})/K|$ for uniformly and randomly

distributed phase values ($\phi^{(k)} \in [0, 2\pi]$), which is $\sqrt{3/K}$.[77] We verified this theoretical 95% threshold for MSPC by a Monte Carlo simulation. We computed MSPC from surrogate data of uniformly and randomly distributed phase values of $\tilde{\Delta}\phi_{XY}^{(k)}$. We repeated this procedure 10,000 times to obtain the statistical distribution of MSPC values for different number of samples in the test set, $K(K = 50, 100, \ldots, 1000)$. An example of the distribution of MSPC ($K = 600$) is shown in Fig. B.1(a) The 95% confidence threshold is 0.0707, which is equivalent to the theoretical value $\sqrt{3/600}$. Figure B.1(b) shows the theoretical predictions and simulation results of 95% confidence threshold for our tests. It can be observed that the theoretical predictions are consistent with the simulation results.

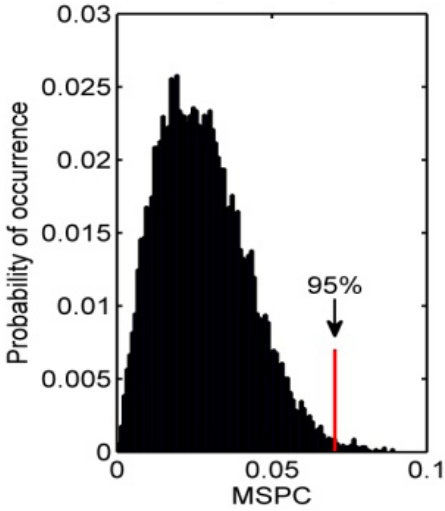

(a) An example of MSPC distribution (K = 600)

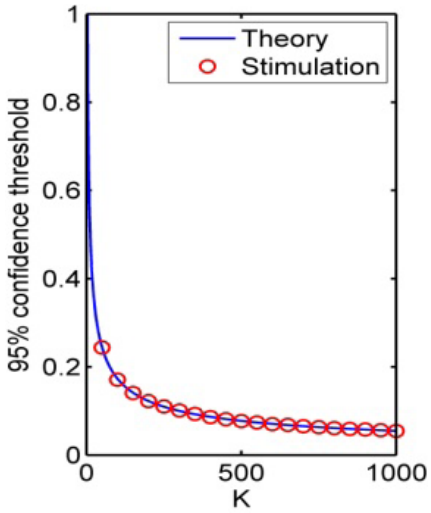

(b) 95% confidence threshold for different number of samples (K)

Fig. B.1. (Color online) Confidence threshold of MSPC. (a) Example of the distribution of MSPC for simulated data ($K = 600$). The red line indicates the 95% confidence threshold. (b) Comparison with the theoretical 95% confidence threshold (blue line) of MSPC for different number of epochs (K) and the results of our simulation (red circles).

Appendix C. Robustness to Noise

To test the robustness of MSPC to noise, we performed a series of simulations with different levels of SNR (SNR $= 0, -5, -10, -15, -20, -25, -30, -35, -40$ dB). Using $x(t)$ and $y(t)$ as the input and the output of a nonlinear system: $y = x^d(t - \tau)$, and $X(f)$ and $Y(f)$ as their Fourier transforms. We use the same input signal as in Sec. 3, a multisine signal with 7, 13 and 29 Hz and a stimulated third-order nonlinear system with the time delay 29.3 ms. All simulations considered 600 periods of the system input. To guarantee the same SNR in all frequency components generated by the nonlinear system, we normalized the power of $Y(f)$ at these frequencies by $Y(f) = Y(f)/|Y(f)|$ and obtained the new $y(t)$ by inverse Fourier transform. Note that this process does not change the phase of any frequency component. Independent white noise signals were added to $x(t)$ and the new $y(t)$ to get the noise-contaminated input and output. Afterwards, we computed MSPC between the noisy input and output for all different SNR. The time delay was estimated using only the frequency components with significant MSPC values. Figure C.1. shows MSPC, estimated phase lags and time delay error for different SNR. The time delay error indicates the difference between the estimated time delay and the true time delay. As the SNR decreases, the mean significant MSPC over frequencies drops and the time delay error increases. Significant MSPC are not shown in all frequency combinations when the SNR decreases below −35 dB. Additionally, the time delay error has a sharp increase as the SNR decreases below −35 dB. These results indicate that MSPC reliably detects nonlinear interactions when the SNR is higher than −35 dB.

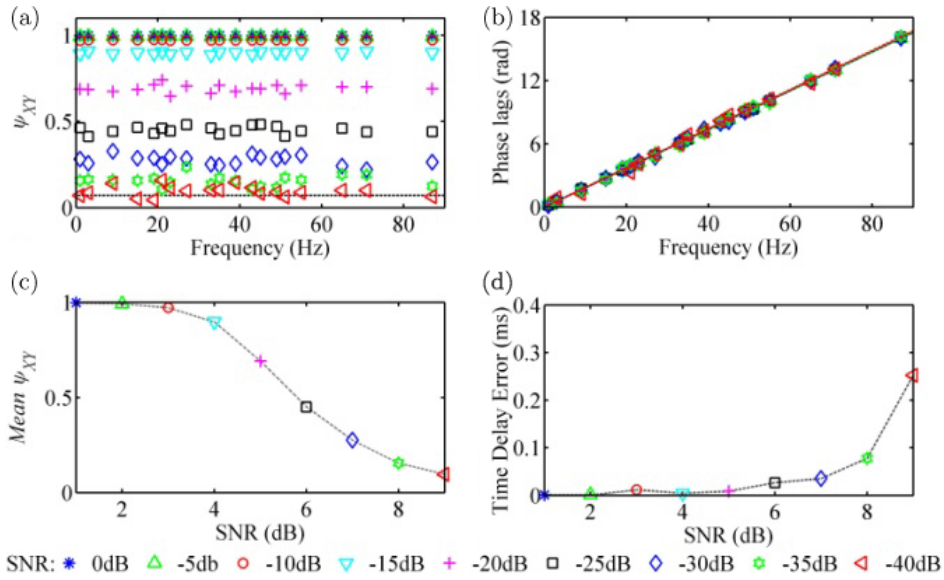

Fig. C.1. Estimated nonlinear interaction for varying SNR. (a) MSPC for harmonics and intermodulations in the third order. The horizontal line indicates the 95% confidence threshold. (b) Estimated phase lags and the lines with the slope. (c) Mean over frequency combinations. (d) Time delay error.

References

1. J. Bhattacharya, H. Petsche and E. Pereda, Long-range synchrony in the γ band: Role in music perception, *J. Neurosci.* **21**(16) (2001) 6329–6337.
2. C.-C. Chen, J. M. Kilner, K. J. Friston, S. J. Kiebel, R. K. Jolly and N. S. Ward, Nonlinear coupling in the human motor system, *J. Neurosci.* **30**(25) (2010) 8393–8399.
3. F. Darvas, K. J. Miller, R. P. Rao and J. G. Ojemann, Nonlinear phase–phase cross-frequency coupling mediates communication between distant sites in human neocortex, *J. Neurosci.* **29**(2) (2009) 426–435.
4. F. Varela, J.-P. Lachaux, E. Rodriguez and J. Martinerie, The brainweb: Phase synchronization and large-scale integration, *Nat. Rev. Neurosci.* **2**(4) (2001) 229–239.
5. T. Womelsdorf, J.-M. Schoffelen, R. Oostenveld, W. Singer, R. Desimone, A. K. Engel and P. Fries, Modulation of neuronal interactions through neuronal synchronization, *Science* **316**(5831) (2007) 1609–1612.
6. S. F. Campfens, A. C. Schouten, M. J. van Putten and H. van der Kooij, Quantifying connectivity via efferent and afferent pathways in motor control using coherence measures and joint position perturbations, *Exp. Brain Res.* **228**(2) (2013) 141–153.
7. R. Srinivasan, W. R. Winter, J. Ding and P. L. Nunez, EEG and MEG coherence: Measures of functional connectivity at distinct spatial scales of neocortical dynamics, *J. Neurosci. Methods* **166**(1) (2007) 41–52.
8. D. Tucker, D. Roth and T. Bair, Functional connections among cortical regions: Topography of EEG coherence, *Electroencephalogr. Clin. Neurophysiol.* **63**(3) (1986) 242–250.
9. J.-M. Schoffelen, R. Oostenveld and P. Fries, Neuronal coherence as a mechanism of effective corticospinal interaction, *Science* **308**(5718) (2005) 111–113.
10. C. Chen, S. J. Kiebel and K. J. Friston, Dynamic causal modelling of induced responses, *Neuroimage* **41**(4) (2008) 1293–1312.
11. D. Sherman, N. Zhang, S. Garg, N. V. Thakor, M. A. Mirski, M. A. White and M. J. Hinich, Detection of nonlinear interactions of EEG alpha waves in the brain by a new coherence measure and its application to epilepsy and anti-epileptic drug therapy, *Int. J. Neural Syst.* **21**(2) (2011) 115–126.
12. M. Ahmadlou and H. Adeli, Functional community analysis of brain: A new approach for EEG-based investigation of the brain pathology, *Neuroimage* **58**(2) (2011) 401–408.
13. M. Ahmadlou and H. Adeli, Fuzzy synchronization likelihood with application to attention-deficit/hyperactivity disorder, *Clin. EEG Neurosci.* **42**(1) (2011) 6–13.
14. K. J. Friston, Brain function, nonlinear coupling, and neuronal transients, *neuroscientist* **7**(5) (2001) 406–418.
15. K. J. Friston, The labile brain. I. Neuronal transients and nonlinear coupling, *Philos. Trans. R. Soc. Lond. B.* **355**(1394) (2000) 215–236.
16. C. S. Herrmann, Human EEG responses to 1–100 Hz flicker: Resonance phenomena in visual cortex and

their potential correlation to cognitive phenomena, *Exp. Brain Res.* **137**(3–4) (2001) 346–353.
17. S. Tobimatsu, Y. M. Zhang and M. Kato, Steady-state vibration somatosensory evoked potentials: Physiological characteristics and tuning function, *Clin. Neurophysiol.* **110**(11) (1999) 1953–1958.
18. X. Chen, Z. Chen, S. Gao and X. Gao, Brain–computer interface based on intermodulation frequency, *J. Neural Eng.* **10**(6) (2013) 066009.
19. A. S. Giani, E. Ortiz, P. Belardinelli, M. Kleiner, H. Preissl and U. Noppeney, Steady-state responses in MEG demonstrate information integration within but not across the auditory and visual senses, *Neuroimage* **60**(2) (2012) 1478–1489.
20. C. Hou, M. W. Pettet, V. Sampath, T. R. Candy and A. M. Norcia, Development of the spatial organization and dynamics of lateral interactions in the human visual system, *J. Neurosci.* **23**(25) (2003) 8630–8640.
21. M. A. Belluscio, K. Mizuseki, R. Schmidt, R. Kempter and G. Buzsáki, Cross-frequency phase–phase coupling between theta and gamma oscillations in the hippocampus, *J. Neurosci.* **32**(2) (2012) 423–435.
22. R. T. Canolty and R. T. Knight, The functional role of cross-frequency coupling, *Trends Cogn. Sci.* **14**(11) (2010) 506–515.
23. O. Jensen and L. L. Colgin, Cross-frequency coupling between neuronal oscillations, *Trends Cogn. Sci.* **11**(7) (2007) 267–269.
24. R. Greenblatt, M. Pflieger and A. Ossadtchi, Connectivity measures applied to human brain electrophysiological data, *J. Neurosci. Methods* **207**(1) (2012) 1–16.
25. V. V. Nikouline, K. Linkenkaer-Hansen, J. Huttunen and R. J. Ilmoniemi, Interhemispheric phase synchrony and amplitude correlation of spontaneous beta oscillations in human subjects: A magnetoencephalographic study, *Neuroreport* **12**(11) (2001) 2487–2491.
26. S. Vanhatalo, J. M. Palva, M. Holmes, J. Miller, J. Voipio and K. Kaila, Infraslow oscillations modulate excitability and interictal epileptic activity in the human cortex during sleep, *Proc. Nat. Acad. Sci. USA.* **101**(14) (2004) 5053–5057.
27. R. T. Canolty, E. Edwards, S. S. Dalal, M. Soltani, S. S. Nagarajan, H. E. Kirsch, M. S. Berger, N. M. Barbaro and R. T. Knight, High gamma power is phase-locked to theta oscillations in human neocortex, *Science* **313**(5793) (2006) 1626–1628.
28. P. Sauseng and W. Klimesch, What does phase information of oscillatory brain activity tell us about cognitive processes? *Neurosci. Biobehav. Rev.* **32**(5) (2008) 1001–1013.
29. C. K. Young and J. J. Eggermont, Coupling of mesoscopic brain oscillations: Recent advances in analytical and theoretical perspectives, *Prog. Neurobiol.* **89**(1) (2009) 61–78.
30. K. Hasselmann, W. Mubk and G. MacDonald, Bispectra of ocean waves, in *Time Series Analysis*, ed. M. Rodenblatt (John Wiley, New York, 1963), pp. 125–139.
31. C. L. Nikias and M. R. Raghuveer, Bispectrum estimation: A digital signal processing framework, *Proc. IEEE* **75**(7) (1987) 869–891.
32. D. L. Sherman and M. D. Zoltowski, Matrix-based higher order spectral analysis for three-wave coupling processes, *IEEE Trans. Signal Process.* **42**(2) (1994) 332–348.
33. F. Chella, L. Marzetti, V. Pizzella, F. Zappasodi and G. Nolte, Third order spectral analysis robust to mixing artifacts for mapping cross-frequency interactions in EEG/MEG, *Neuroimage* **91** (2014) 146–161.
34. H. He and D. J. Thomson, Canonical bicoherence analysis of dynamic EEG data, *J. Comput. Neurosci.* **29**(1–2) (2010) 23–34.
35. T. Schanze and R. Eckhorn, Phase correlation among rhythms present at different frequencies: Spectral methods, application to microelectrode recordings from visual cortex and functional implications, *Int. J. Psychophysiol.* **26**(1–3) (1997) 171–189.
36. A. Von Stein, C. Chiang and P. König, Top-down processing mediated by interareal synchronization, *Proc. Nat. Acad. Sci. USA.* **97**(26) (2000) 14748–14753.
37. J. Shils, M. Litt, B. Skolnick and M. Stecker, Bispectral analysis of visual interactions in humans, *Electroencephalogr. Clin. Neurophysiol.* **98**(2) (1996) 113–125.
38. U. R. Acharya, E. C.-P. Chua, K. C. Chua, L. C. Min and T. Tamura, Analysis and automatic identification of sleep stages using higher order spectra, *Int. J. Neural Syst.* **20**(6) (2010) 509–521.
39. J. Muthuswamy, D. L. Sherman and N. V. Thakor, Higher-order spectral analysis of burst patterns in EEG, *IEEE Trans. Biomed. Eng.* **46**(1) (1999) 92–99.
40. J. C. Sigl and N. G. Chamoun, An introduction to bispectral analysis for the electroencephalogram, *J. Clin. Monit.* **10**(6) (1994) 392–404.
41. Z. Vahabi, R. Amirfattahi, F. Shayegh and F. Ghassemi, Online epileptic seizure prediction using wavelet-based bi-phase correlation of electrical signals tomography, *Int. J. Neural Syst.* **25**(6) (2015) 15500288.
42. F. Darvas, J. G. Ojemann and L. B. Sorensen, Bi-phase locking — A tool for probing non-linear interaction in the human brain, *Neuroimage* **46**(1) (2009) 123–132.
43. J.-P. Lachaux, E. Rodriguez, J. Martinerie and F. J. Varela, Measuring phase synchrony in brain signals, *Hum. Brain Mapp.* **8**(4) (1999) 194–208.

44. P. Tass, M. Rosenblum, J. Weule, J. Kurths, A. Pikovsky, J. Volkmann, A. Schnitzler and H.-J. Freund, Detection of $n:m$ phase locking from noisy data: Application to magnetoencephalography, *Phys. Rev. Lett.* **81**(15) (1998) 3291.
45. I. Clark, R. Biscay, M. Echeverría and T. Virués, Multiresolution decomposition of non-stationary EEG signals: A preliminary study, *Comput. Biol. Med.* **25**(4) (1995) 373–382.
46. F. Mormann, K. Lehnertz, P. David and C. E. Elger, Mean phase coherence as a measure for phase synchronization and its application to the EEG of epilepsy patients, *Physica D* **144**(3) (2000) 358–369.
47. D. Serletis, P. L. Carlen, T. A. Valiante and B. L. Bardakjian, Phase synchronization of neuronal noise in mouse hippocampal epileptiform dynamics, *Int. J. Neural Syst.* **23**(1) (2013) 1250033.
48. J. M. Palva, S. Palva and K. Kaila, Phase synchrony among neuronal oscillations in the human cortex, *J. Neurosci.* **25**(15) (2005) 3962–3972.
49. M. Regan and D. Regan, A frequency domain technique for characterizing nonlinearities in biological systems, *J. Theor. Biol.* **133**(3) (1988) 293–317.
50. S. Jamali and B. Ross, Somatotopic finger mapping using MEG: Toward an optimal stimulation paradigm, *Clin. Neurophysiol.* **124**(8) (2013) 1659–1670.
51. B. Ross, S. Jamali, T. Miyazaki and T. Fujioka, Synchronization of beta and gamma oscillations in the somatosensory evoked neuromagnetic steady-state response, *Exp. Neurol.* **245** (2013) 40–51.
52. J. Victor and R. Shapley, A method of nonlinear analysis in the frequency domain, *Biophys. J.* **29**(3) (1980) 459.
53. M. G. Rosenblum, A. S. Pikovsky and J. Kurths, Phase synchronization of chaotic oscillators, *Phys. Rev. Lett.* **76**(11) (1996) 1804.
54. G. Zhou and G. B. Giannakis, Retrieval of self-coupled harmonics, *IEEE Trans. Signal Process.* **43**(5) (1995) 1173–1186.
55. C. W. J. Granger, Investigating causal relations by econometric models and cross-spectral methods, *Econometrica* **37**(3) (1969) 424–438.
56. C. L. Witham, C. N. Riddle, M. R. Baker and S. N. Baker, Contributions of descending and ascending pathways to corticomuscular coherence in humans, *J. Physiol.* **589**(15) (2011) 3789–3800.
57. A. J. Langdon, T. W. Boonstra and M. Breakspear, Multi-frequency phase locking in human somatosensory cortex, *Prog. Biophys. Mol. Biol.* **105**(1) (2011) 58–66.
58. Q. Zhang, K. R. Lutchen and B. Suki, A frequency domain approach to nonlinear and structure identification for long memory systems: Application to lung mechanics, *Ann. Biomed. Eng.* **27**(1) (1999) 1–13.
59. T. Ball, M. Kern, I. Mutschler, A. Aertsen and A. Schulze-Bonhage, Signal quality of simultaneously recorded invasive and non-invasive EEG, *Neuroimage* **46**(3) (2009) 708–716.
60. G. Lu, J.-S. Brittain, P. Holland, J. Yianni, A. L. Green, J. F. Stein, T. Z. Aziz and S. Wang, Removing ECG noise from surface EMG signals using adaptive filtering, *Neurosci. Lett.* **462**(1) (2009) 14–19.
61. A. Z. Snyder, Steady-state vibration evoked potentials: Description of technique and characterization of responses, *Electroencephalogr. Clin. Neurophysiol.* **84**(3) (1992) 257–268.
62. S. Hagihira, M. Takashina, T. Mori, T. Mashimo and I. Yoshiya, Practical issues in bispectral analysis of electroencephalographic signals, *Anesth. Analg.* **93**(4) (2001) 966–970.
63. S. Kalitzin, J. Parra, D. N. Velis and F. Silva, Enhancement of phase clustering in the EEG/MEG gamma frequency band anticipates transitions to paroxysmal epileptiform activity in epileptic patients with known visual sensitivity, *IEEE Trans. Biomed. Eng.* **49**(11) (2002) 1279–1286.
64. A. Hutt, A. Daffertshofer and U. Steinmetz, Detection of mutual phase synchronization in multivariate signals and application to phase ensembles and chaotic data, *Phys. Rev. E* **68**(3) (2003) 036219.
65. K. J. Friston, Functional and effective connectivity in neuroimaging: A synthesis, *Hum. Brain Mapp.* **2**(12) (1994) 56–78.
66. M. Rubinov and O. Sporns, Complex network measures of brain connectivity: Uses and interpretations, *Neuroimage* **52**(3) (2010) 1059–1069.
67. F. L. da Silva, J. P. Pijn and P. Boeijinga, Interdependence of EEG signals: Linear vs. nonlinear associations and the significance of time delays and phase shifts, *Brain Topogr.* **2**(1–2) (1989) 9–18.
68. R. Govindan, J. Raethjen, F. Kopper, J. Claussen and G. Deuschl, Estimation of time delay by coherence analysis, *Physica A* **350**(2) (2005) 277–295.
69. D. R. Stapells, S. Makeig and R. Galambos, Auditory steady-state responses: Threshold prediction using phase coherence, *Electroencephalogr. Clin. Neurophysiol.* **67**(3) (1987) 260–270.
70. S. Makeig, M. Westerfield, T.-P. Jung, S. Enghoff, J. Townsend, E. Courchesne and T. Sejnowski, Dynamic brain sources of visual evoked responses, *Science* **295**(5555) (2002) 690–694.
71. A. L. Hume and B. Cant, Conduction time in central somatosensory pathways in man, *Electroencephalogr. Clin. Neurophysiol.* **45**(3) (1978) 361–375.
72. H. Hämäläinen, J. Kekoni, M. Sams, K. Reinikainen and R. Näätänen, Human somatosensory evoked potentials to mechanical pulses and vibration: Contributions of SI and SII somatosensory cortices to P50 and P100 components, *Electroencephalogr. Clin. Neurophysiol.* **75**(1) (1990) 13–21.
73. T. Mima and M. Hallett, Corticomuscular coherence: A review, *J. Clin. Neurophysiol.* **16**(6) (1999) 501.

74. S.-H. Jin, P. Lin and M. Hallett, Linear and nonlinear information flow based on time-delayed mutual information method and its application to corticomuscular interaction, *Clin. Neurophysiol.* **121**(3) (2010) 392–401.
75. F. Meng, K.-Y. Tong, S.-T. Chan, W.-W. Wong, K.-H. Lui, K.-W. Tang, X. Gao and S. Gao, Study on connectivity between coherent central rhythm and electromyographic activities, *J. Neural. Eng.* **5**(3) (2008) 324.
76. C. J. Stam, G. Nolte and A. Daffertshofer, Phase lag index: Assessment of functional connectivity from multi channel EEG and MEG with diminished bias from common sources, *Hum. Brain Mapp.* **28**(11) (2007) 1178–1193.
77. J. L. Shils, The bispectrum of the human electroencephalogram, PhD thesis, University of Pennsylvania, Philadelphia, PA (1995).